

**CHEMICAL ENGINEERING DIVISION
FUELS AND MATERIALS CHEMISTRY
SEMIANNUAL REPORT**

January—June 1971

**P. E. Blackburn, C. E. Johnson, J. E. Battles,
I. Johnson, A. E. Martin, M. Tetenbaum,
C. E. Crouthamel, A. D. Tevebaugh, and R. C. Vogel**



U of C-AIA-USAEC

ARGONNE NATIONAL LABORATORY, ARGONNE, ILLINOIS

The facilities of Argonne National Laboratory are owned by the United States Government. Under the terms of a contract (W-31-109-Eng-38) between the U. S. Atomic Energy Commission, Argonne Universities Association and The University of Chicago, the University employs the staff and operates the Laboratory in accordance with policies and programs formulated, approved and reviewed by the Association.

MEMBERS OF ARGONNE UNIVERSITIES ASSOCIATION

The University of Arizona	Kansas State University	The Ohio State University
Carnegie-Mellon University	The University of Kansas	Ohio University
Case Western Reserve University	Loyola University	The Pennsylvania State University
The University of Chicago	Marquette University	Purdue University
University of Cincinnati	Michigan State University	Saint Louis University
Illinois Institute of Technology	The University of Michigan	Southern Illinois University
University of Illinois	University of Minnesota	The University of Texas at Austin
Indiana University	University of Missouri	Washington University
Iowa State University	Northwestern University	Wayne State University
The University of Iowa	University of Notre Dame	The University of Wisconsin

NOTICE

This report was prepared as an account of work sponsored by the United States Government. Neither the United States nor the United States Atomic Energy Commission, nor any of their employees, nor any of their contractors, subcontractors, or their employees, makes any warranty, express or implied, or assumes any legal liability or responsibility for the accuracy, completeness or usefulness of any information, apparatus, product or process disclosed, or represents that its use would not infringe privately-owned rights.

Printed in the United States of America
Available from
National Technical Information Service
U.S. Department of Commerce
5285 Port Royal Road
Springfield, Virginia 22151
Price: Printed Copy \$3.00; Microfiche \$0.95

ARGONNE NATIONAL LABORATORY
9700 South Cass Avenue
Argonne, Illinois 60439

CHEMICAL ENGINEERING DIVISION
FUELS AND MATERIALS CHEMISTRY
SEMIANNUAL REPORT

January-June 1971

by

P. E. Blackburn, C. E. Johnson, J. E. Battles,
I. Johnson, A. E. Martin, M. Tetenbaum,
C. E. Crouthamel, A. D. Tevebaugh, and R. C. Vogel

September 1971

TABLE OF CONTENTS

	<u>Page</u>
ABSTRACT.	1
SUMMARY	2
I. MATERIALS CHEMISTRY AND THERMODYNAMICS.	4
A. Thermodynamic Equilibrium Studies of the Na-U-O System by Mass Spectrometry.	4
B. The U-Pu-O, Na-U-O and Na-U-Pu-O Phase Studies	10
1. The Na-U-O Phase Study.	10
2. The Study of the Na-U-Pu-O System	13
C. Studies of the U-Mo-O System	15
D. Studies of the U-Pu-O System Containing Fission Products	16
E. Thermodynamics of Carbide Fuels: Vaporization Behavior of the U-C-O System	18
II. CHEMISTRY OF IRRADIATED FUELS AND MATERIALS	23
A. Fission-Product Distribution in Mixed-Oxide Fuels. . .	23
1. Radial Distribution of Krypton.	23
2. Radial Distribution of Cesium	25
B. Fuel-Cladding Chemical Interactions.	25
REFERENCES.	32

LIST OF FIGURES

<u>No.</u>	<u>Title</u>	<u>Page</u>
I-1	Portion of Na-U-O Phase Diagram Showing Composition Calculated for Each Experiment.	6
I-2	Na ₃ Mo ₄ Phase Formed from Reaction of 20% PuO ₂ -80% UO ₂ Sintered Pellet with Liquid Sodium at 900°C.	14
I-3	Partial Phase Diagram of U-Cs-O System	17
I-4	Tentative Phase Diagram of U-C-O System at ~1700°C	22
II-1	Radial Distribution of ⁸⁵ Kr in Irradiated Mixed-Oxide Fuel (HOV-15)	24
II-2	Radial Distribution of ¹³⁷ Cs in Irradiated Mixed-Oxide Fuels.	26
II-3	Electron Microprobe Scanning Images of Irradiated Stainless Steel Cladding from SOV-1.	29
II-4	Electron Microprobe Analysis of an Area of Intergranular Attack in Irradiated Stainless Steel Cladding (SOV-1).	30

LIST OF TABLES

<u>No.</u>	<u>Title</u>	<u>Page</u>
I-1	Data on Preparations of Na ₃ UO ₄	12
I-2	Reactions of Cs ₂ O and Cesium with Urania	19
I-3	Composition and Phase Transformation Traverse via Controlled Oxygen and Carbon Potentials in Carrier Gas.	21
II-1	Oxygen Content of Irradiated Stainless Steel Cladding.	28

CHEMICAL ENGINEERING DIVISION
FUELS AND MATERIALS CHEMISTRY
SEMIANNUAL REPORT

January-June 1971

by

P. E. Blackburn, C. E. Johnson, J. E. Battles,
I. Johnson, A. E. Martin, M. Tetenbaum,
C. E. Crouthamel, A. D. Tevebaugh, and R. C. Vogel

ABSTRACT

To aid in evaluating the performance of fast-breeder reactor fuels, high-temperature investigations are being made of the U-Pu-O-Na, U-Pu-O-Cs, U-Mo-O, and U-C-O systems, and the chemical behavior of irradiated fuels is being investigated.

Mass-spectrometric and phase studies of the U-O-Na and U-Pu-O-Na systems are being directed toward determining conditions under which a reaction between oxide fuels and sodium coolant can be prevented. Mass-spectrometric studies of the U-Mo-O system are being conducted to aid in understanding the migration of fission-product molybdenum and fuel-cladding interactions that occur in irradiated oxide fuels. Phase relationships of the U-Pu-O-Cs system are being investigated to establish conditions under which fission-product cesium interacts with mixed-oxide fuel during irradiation and to obtain data useful in the development of an understanding of the irradiated fuel-cladding interactions. Activity measurements in the U-C-O system have been made by a gas-equilibration and transpiration technique to determine the effects of oxygen contamination on the performance of carbide fuels.

Studies have been made of the distribution of fission products in irradiated UO_2 -20 wt % PuO_2 fuels. Data are presented on the radial distribution of ^{85}Kr in vibratorily compacted fuel, and a comparison is made of the radial distribution of ^{137}Cs in vibratorily compacted and high-density pellet fuels.

Recent work has indicated that in irradiated mixed-oxide fuels the mechanism of attack of the cladding is oxidation at the grain boundaries. Microprobe examination of specimens of stainless steel cladding has shown the presence of oxygen as well as cesium and molybdenum in areas of intergranular attack.

SUMMARY

Materials Chemistry and Thermodynamics

The information obtained in this program can be used to interpret and evaluate the performance of fast-breeder-reactor fuels. The reaction of $(U,Pu)O_2$ fuel with sodium coolant, in the event of a cladding failure, could cause serious problems in reactor operation. Studies are being conducted to identify the products of sodium-fuel reactions, to determine oxygen and sodium partial pressures in equilibrium with the products, and to establish the conditions under which reaction does not occur.

Thermodynamic Equilibrium Studies of the Na-U-O System. A mass-spectrometric thermodynamic study of the Na-U-O system has been carried out to establish oxygen pressures in equilibrium with the three-phase system $Na-UO_2-Na_3UO_4$. The oxygen pressure may be used to determine oxygen content of UO_2 and Na. The oxygen pressure was not obtained directly, but may be calculated from sodium pressures measured from three-phase Na-U-O regions adjacent to the $Na-UO_2-Na_3UO_4$ region and oxygen pressure measured in one of the four regions. If the calculated oxygen pressure in equilibrium with the $Na-UO_2-Na_3UO_4$ is the same as that in equilibrium with $Na-U_{0.8}Pu_{0.2}O_2-Na_3U_{1-y}Pu_yO_4$, these data indicate an O/M ratio for $U_{0.8}Pu_{0.2}O_{2-x}$ of about 1.96 at 1200°K.

The U-Pu-O, Na-U-O and Na-U-Pu-O Phase Studies. Studies of the Na-U-O system confirmed that Na_3UO_4 is the phase in equilibrium with Na and UO_2 . Several additional equilibrium triangles were also established in the Na-U-O system. $Na_3U_{1-y}Pu_yO_4$ was identified by X-ray diffraction as the product of the reaction at 900°C of sodium with a sintered pellet of composition $U_{0.8}Pu_{0.2}O_{1.995}$. A calculation based on the weight change of a pellet after 20 days at 900°C indicated that the O/M composition of the product mixed-oxide phase was 1.95.

Studies of the U-Mo-O System. The effects of molybdenum on the oxygen potentials in the U-Mo-O system are being investigated. Oxygen potentials, molybdenum oxide pressures, and X-ray data indicate an interaction between Mo and UO_{2+x} .

Studies of the U-Pu-O System Containing Fission Products. The interaction of Cs with UO_2 is being investigated. Cs_2UO_4 has been identified as one of the products formed between Cs_2O and UO_2 . Pressures are being measured over the U-Cs-O system to establish the thermodynamic properties of the system.

Thermodynamics of Carbide Fuels: Transpiration Studies of the U-C-O System. Oxygen and carbon potentials have been measured in single-phase UC_xO_y and three-phase $UC_xO_y-UC_2-UO_2$.

Chemistry of Irradiated Fuels and Materials

The chemical behavior of irradiated fast-reactor fuels is being studied in order to understand the complex processes that occur in these

fuels during irradiation. Data on the retention and distribution of noble-gas fission products in irradiated fuels are needed for the development of fuel-swelling models. An understanding of the mechanisms of fuel-cladding interactions will aid in producing fuels with long lifetimes.

Fission-Product Distribution in Mixed-Oxide Fuels. The radial distribution of residual ^{85}Kr in an irradiated mixed-oxide fuel (HOV-15) has been determined by a combination of laser-beam sampling and beta counting. The amount of ^{85}Kr in the columnar grain region near the central void was found to be larger than in the cooler end of the columnar grains and in the equiaxed grain region. Mechanisms are proposed to account for the observed behavior.

The radial distribution of ^{137}Cs has been determined by laser-beam sampling and gamma spectrometry. The results show that the behavior of ^{137}Cs differs in vibratorily compacted fuel (HOV-15 and SOV-6) and high-density pellet fuel (F2R). In the high-density fuel, little cesium migration to the fuel-cladding interface was observed, whereas in the lower density vibrapacked fuels, the cesium concentration was highest near the fuel-cladding interface.

Fuel-Cladding Chemical Interactions. Analyses of irradiated fuel-cladding specimens for oxygen have shown the cladding to contain up to 0.3% oxygen. This concentration is significantly higher than in unirradiated material (50 to 97 ppm). Electron microprobe examinations of the specimens have shown large concentrations of oxygen in the cladding grain boundaries as well as the presence of cesium and molybdenum. A possible mechanism of attack is the accelerated oxidation (similar to hot corrosion) of the cladding grain boundary.

I. MATERIALS CHEMISTRY AND THERMODYNAMICS (P. E. Blackburn)

The objective of this program is to obtain phase-diagram, thermodynamic, and chemical data that can be used to interpret and evaluate the performance of fast-breeder-reactor fuels. This information will aid in understanding and in selecting methods for control of sodium-fuel interactions, fission product distribution in the fuel, cladding attack by corrosive fission products, plutonium segregation, and fuel swelling. In addition, these data will help to identify phases formed in fuel under operating conditions and to choose additives for controlling the chemical potentials of fuel anions and those fission products which are deleterious to prolonged fuel-pin lifetimes.

A. Thermodynamic Equilibrium Studies of the Na-U-O System by Mass Spectrometry (J. E. Battles, W. A. Shinn)

Mass-spectrometric studies of the volatilization behavior of the uranium-plutonium-oxygen system have been directed toward determining the parent vapor species in equilibrium with the condensed phase(s), partial pressures of the vapor species as a function of temperature and composition, and thermodynamic properties. A study of the volatilization behavior of single-phase $(U_{0.8}Pu_{0.2})O_{2-x}$ material has been reported.¹ Present studies are directed toward obtaining oxygen and sodium partial pressures in equilibrium with the compounds resulting from the reaction of liquid sodium with oxide fuel materials [i.e., $(U,Pu)O_2$]; this information may be useful in establishing the conditions necessary to prevent sodium-fuel reaction. Mass-spectrometric experiments have been conducted to determine the oxygen partial pressure in equilibrium with the three-phase system $Na-UO_2-Na_3UO_4$. Subsequent experiments are scheduled to include the compounds Na_3PuO_4 and/or $Na_3(U,Pu)O_4$.

The mass spectrometer normally has a sensitivity or detection limit of about 10^{-9} atm (vapor pressure of species effusing from an effusion cell); however, because of interference by the normal oxygen background of the vacuum system, effusion-cell pressure must be $>10^{-7}$ atm to detect oxygen effusing from the cell. Since the oxygen partial pressure (P_{O_2}) in equilibrium with $Na-UO_2-Na_3UO_4$ was expected to be very low, it was considered necessary to find some other procedure for determining P_{O_2} . Preliminary experiments with Na_2O-UO_2 indicated that vapor species to be expected from dissociation of Na_3UO_4 are $Na(g)$, $Na_2(g)$, $NaO(g)$, $Na_2O(g)$, and $O_2(g)$. Accordingly, experiments with the vaporization of $Na_2O(s)$ and $Na_2WO_4(s)$ were conducted in an effort to find oxygen-containing molecules which could be used for obtaining P_{O_2} by means of a vapor-phase reaction such as $Na(g) + 1/2 O_2(g) \rightleftharpoons NaO(g)$. However, these experiments were unsuccessful since disodium oxide (Na_2O) vaporized predominantly as $Na(g)$ and $O_2(g)$ with only a very minor amount of $Na_2O(g)$ (NaO not detected). Na_2O pressures were not sufficient for quantitative measurements. Similarly, the sodium tungstate (Na_2WO_4) vaporized as $Na(g)$ (very strong), $Na_2WO_4(g)$ (medium), and $Na_2O(g)$ (very weak).

Because of the failure of the above approaches to establish a calibration procedure, a small sample (~ 175 mg) of Na_3UO_4 (91 mol % Na_3UO_4 , 9 mol % UO_2) was heated in an iridium effusion cell (tungsten outer cell), and, as Na_3UO_4 dissociated, the vapor species were observed to determine if normal dissociation would permit direct measurement of the P_{O_2} . During the initial dissociation and at low temperatures ($< \sim 900^\circ\text{C}$), Na(g) was the only vapor species detected. At higher temperatures ($> \sim 1000^\circ\text{C}$) and after considerable vaporization of Na(g) , the vapor phase was Na(g) and $\text{O}_2(\text{g})$; no other vapor species were detected.

Because of the success of the above experiment, a series of controlled experiments were conducted to identify the three-phase region suitable for measuring partial pressures of Na and O_2 as well as to determine Na pressures of the intermediate three-phase regions. The same material as that used above (~ 600 mg) was heated in an iridium effusion cell for about 4 hr in each experiment, each experiment being conducted at a higher temperature than the preceding experiment. Temperature was measured with an optical pyrometer, and an accurate account was kept of the total weight loss of the sample. Also, samples were taken for X-ray diffraction analysis at the conclusion of each experiment. The vapor pressures were determined from the weight loss and the assumption that the vapor was entirely Na(g) in the earlier experiments ($< 900^\circ\text{C}$), where oxygen was not measurable. In the later experiments, the composition of the vapor phase was determined by assuming equal ionization cross sections for Na^+ and O_2^+ , and the weight loss was proportioned accordingly.

The solid phases were identified by X-ray diffraction analysis at the conclusion of each experiment, and the results demonstrate the dissociation path of Na_3UO_4 by vaporization. The characteristics of this dissociation are more clearly shown in Fig. I-1, a portion of the Na-U-O phase diagram, where the approximate composition is plotted for each experiment. The compositions were calculated from the starting composition, measured weight loss, and the assumption that only sodium was vaporized in the first five experiments. The phase relationships shown in Fig. I-1 were established from the X-ray diffraction analysis. Also, a three-phase region composed of NaUO_3 - $\text{Na}_2\text{U}_2\text{O}_7$ -X was encountered. The phase X is face-centered cubic with lattice parameter $a = 4.3999\text{\AA}$; the molecular formula has not been established.

In this first series of experiments, temperature-dependency and weight-loss measurements were made for Na(g) in the three-phase regions Na_4UO_5 - Na_3UO_4 - NaUO_3 and Na_4UO_5 - NaUO_3 - Na_2UO_4 . Data for both Na(g) and $\text{O}_2(\text{g})$ were obtained in the three-phase region NaUO_3 - Na_2UO_4 - $\text{Na}_2\text{U}_2\text{O}_7$; however, the data for O_2 were somewhat erratic.

A second series of experiments was conducted to establish the reliability of the data acquired in the first series. The tungsten outer cell was replaced with a platinum cell which had a Pt/Pt-10% Rh thermocouple attached to the base for temperature measurements. The thermocouple was calibrated *in situ* against the melting points of high-purity Al, Ag, and Au (1968 International Practical Temperature Scale). Both temperature-dependency and weight-loss measurements for Na(g) agreed very well with

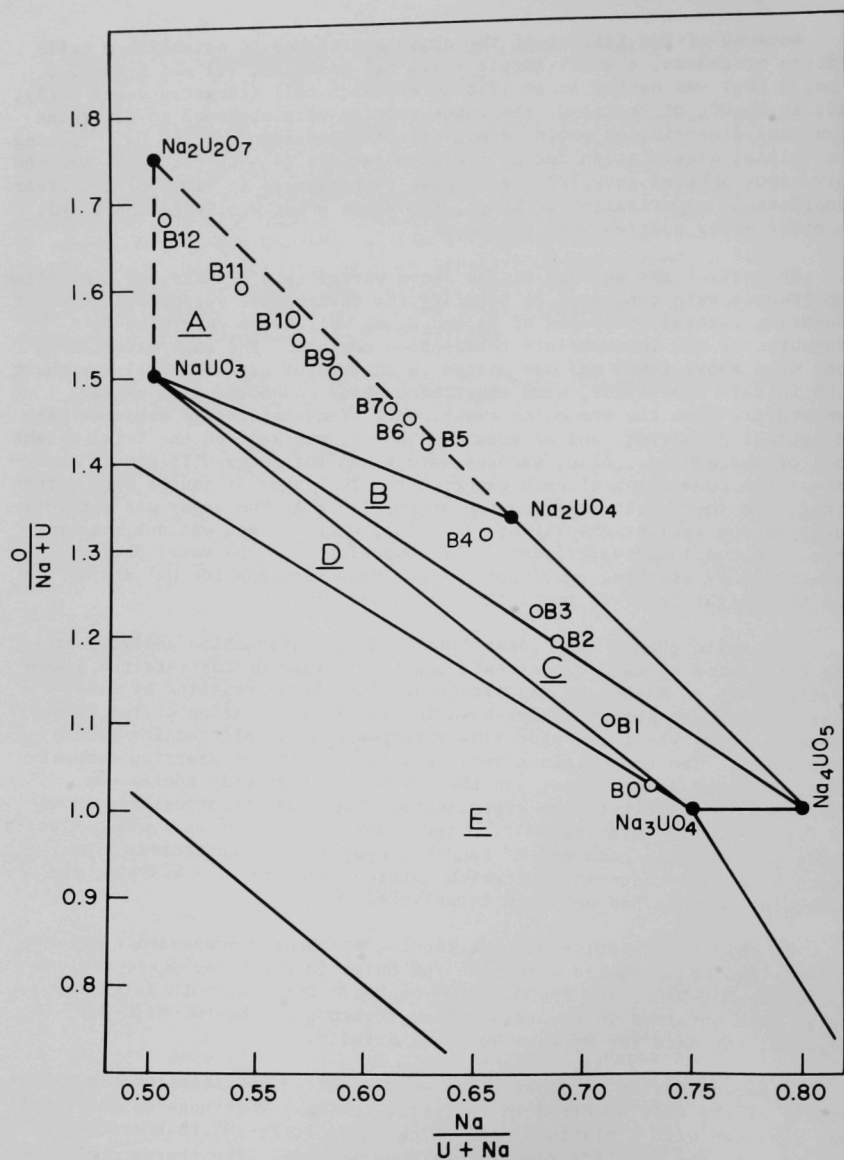


Fig. I-1. Portion of Na-U-O Phase Diagram Showing Composition Calculated for Each Experiment

those obtained in the first series. The data for $O_2(g)$ were reproducible at temperatures less than $1360^\circ K$ and erratic at temperatures above $1360^\circ K$. Since most of the data for $O_2(g)$ in the first series were above $1360^\circ K$, those data were discarded, and only the lower-temperature data of the second series utilized. A third series of experiments was conducted primarily to obtain data for the three-phase region $Na_3UO_4-UO_2-NaUO_3$; previous data were not considered reliable because of the small compositional traverse (see Fig. I-1) which led to data that varied with time at constant temperature. The sample material in this series had initial $O/(U+Na)$ and $Na/(U+Na)$ ratios of 1.09 and 0.68, respectively. The data from this series agreed reasonably well with the previous data for the three-phase regions A, B, and C (Fig. I-1) and were utilized in the evaluation of the pressure-temperature relationships.

For the three-phase region $Na_3UO_4-UO_2-NaUO_3$, the partial enthalpy of vaporization for $Na(g)$ was determined from the slope of the temperature-dependency data (i.e., $\log I^+T$ vs $1/T$, where I^+ is Na^+ intensity). The average value is 63.06 ± 1.14 kcal/mol Na . The partial pressure of $Na(g)$ was determined from the rate-of-effusion (weight-loss) measurements, assuming the vapor phase was entirely $Na(g)$. This is a valid assumption since later calculations show P_{O_2} is about 10^{-12} atm, while an average value of 5.16×10^{-6} atm was obtained for P_{Na} at $1076^\circ K$. When the values for the partial enthalpy and partial pressure at $1076^\circ K$ are used to evaluate the intercept, the following equation is obtained for the pressure-temperature relationship:

$$\log P_{Na} = \frac{-13,780 \pm 250}{T} + 7.520 \quad (837-1085^\circ K) \quad (1)$$

For the three-phase region $Na_3UO_4-Na_4UO_5-NaUO_3$, the following equation is obtained for the pressure-temperature relationship:

$$\log P_{Na} = \frac{-13,790 \pm 420}{T} + 6.850 \quad (1000-1243^\circ K) \quad (2)$$

Similar analysis of the pressure and temperature-dependency data yields the following pressure-temperature relationship for $Na(g)$ in the three-phase region $NaUO_3-Na_2UO_4-Na_4UO_5$:

$$\log P_{Na} = \frac{-13,330 \pm 290}{T} + 6.050 \quad (971-1305^\circ K) \quad (3)$$

For the three-phase region $NaUO_3-Na_2U_2O_7-Na_2UO_4$, the pressure-temperature relationship for $Na(g)$ and $O_2(g)$ can be calculated by two procedures. In the first procedure, the ionization cross sections for $Na(g)$ and $O_2(g)$ are assumed equal, thus permitting the determination of the vapor-phase composition. With this information and the weight-loss data, the partial pressures can be calculated by means of the equation for molecular effusion, i.e.,

$$P_i = \frac{2.256 \times 10^{-2} W F_i \sqrt{\frac{T}{M_i}}}{A t k} \quad (4)$$

where W/At is the rate of effusion in $g/(cm^2)(sec)$, k is the Clausing correction factor, T is the absolute temperature, P_i is the partial pressure, F_i is the weight fraction of total vapor, and M_i is the molecular weight of species i .

In the second procedure, the partial pressures of $Na(g)$ and O_2 can be calculated by determining the constant K , in the relationship

$$I_i^+ T = K P_i \quad (5)$$

where I_i^+ is the measured ion current of a given species. The constant K includes the instrument and geometric factors, the ionization cross section, the multiplier efficiency, and the ionization energy. In this system ($Na-U-O$), we used three three-phase regions ($Na_3UO_4-UO_2-NaUO_3$, $NaUO_3-Na_3UO_4-Na_4UO_5$ and $NaUO_3-Na_4UO_5-Na_2UO_7$) which vaporize almost entirely as $Na(g)$ (P_{O_2} is extremely low) to evaluate K in Eq. 5. The constant K was then used to calculate P_{Na} and P_{O_2} in the region $NaUO_3-Na_4UO_5-Na_2UO_7$. The partial pressure of $Na(g)$ at a given temperature was determined in the first three regions from weight-loss measurements (as noted above). Also, the ion current was measured during these experiments. Additional values of the ion current were obtained from the temperature-dependency data ($\log I_i^+ T$ vs $1/T$). The value of K obtained from all data is $8.73 \times 10^5 \pm \sim 15\%$.

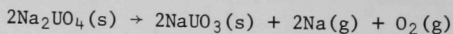
For the three-phase region $NaUO_3-Na_2UO_4-Na_2UO_7$, the partial pressure of $Na(g)$ was calculated from the measured ion intensity I_{Na}^+ obtained during the weight-loss experiments (constant temperature) and the value of K given above. The weight loss due to the vaporization of $Na(g)$ was calculated (Eq. 3), and the weight loss due to the vaporization of $O_2(g)$ was obtained by difference, which permits calculation of P_{O_2} . Applying the same procedure described above (Eq. 1), the following pressure-temperature relationships for $Na(g)$ and $O_2(g)$ were obtained:

$$\log P_{Na} = \frac{-13,960 \pm 600}{T} + 4.940 \quad (1086-1406^\circ K) \quad (6)$$

$$\log P_{O_2} = \frac{-20,300 \pm 580}{T} + 9.500 \quad (1086-1406^\circ K) \quad (7)$$

The partial pressures of $Na(g)$ and $O_2(g)$ obtained by this procedure are independent of any assumptions of the ionization cross-section values. These pressures differ considerably from the pressures calculated earlier, where the ionization cross sections were assumed equal.

The partial pressure of oxygen in equilibrium with Na_3UO_4 , UO_2 , and Na (region E in Fig. I-1) can be calculated from the measured partial pressures of $Na(g)$ and $O_2(g)$ in region A and the P_{Na} measured in regions B, C, D, and E. The reactions involved in these calculations are presented below. In regions A and B, the reaction for $Na_2UO_4(s)$ is



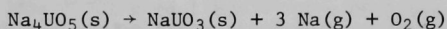
$$\text{Region A: } K_1 = (P_{\text{Na}})_A^2 (P_{\text{O}_2})_A \quad (8)$$

$$\text{Region B: } K_2 = (P_{\text{Na}})_B^2 (P_{\text{O}_2})_B \quad (9)$$

The equilibrium constant K_1 in region A is equal to K_2 in region B; therefore

$$(P_{\text{O}_2})_B = \frac{K_1}{(P_{\text{Na}})_B^2} = \frac{(P_{\text{Na}})_A^2 (P_{\text{O}_2})_A}{(P_{\text{Na}})_B^2} \quad (10)$$

In regions B and C, the reaction for $\text{Na}_4\text{UO}_5(\text{s})$ is



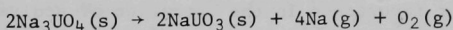
$$\text{Region B: } K_3 = (P_{\text{Na}})_B^3 (P_{\text{O}_2})_B \quad (11)$$

$$\text{Region C: } K_4 = (P_{\text{Na}})_C^3 (P_{\text{O}_2})_C \quad (12)$$

K_3 in region B is equal to K_4 in region C; therefore

$$(P_{\text{O}_2})_C = \frac{K_3}{(P_{\text{Na}})_C^3} = \frac{(P_{\text{Na}})_B^3 (P_{\text{O}_2})_B}{(P_{\text{Na}})_C^3}$$

In regions C and D, the reaction for $\text{Na}_3\text{UO}_4(\text{s})$ is



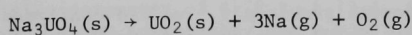
$$\text{Region C: } K_5 = (P_{\text{Na}})_C^4 (P_{\text{O}_2})_C \quad (13)$$

$$\text{Region D: } K_6 = (P_{\text{Na}})_D^4 (P_{\text{O}_2})_D \quad (14)$$

K_5 in region C equals K_6 in region D; therefore

$$(P_{\text{O}_2})_C = \frac{K_5}{(P_{\text{Na}})_D^4} = \frac{(P_{\text{Na}})_C^4 (P_{\text{O}_2})_C}{(P_{\text{Na}})_D^4}$$

In regions D and E, the reaction for $\text{Na}_3\text{UO}_4(\text{s})$ is



$$\text{Region D: } K_7 = (P_{\text{Na}})_D^3 (P_{\text{O}_2})_D \quad (15)$$

$$\text{Region E: } K_8 = (P_{\text{Na}})_E^3 (P_{\text{O}_2})_E \quad (16)$$

K_7 in region D equals K_8 in region E; therefore

$$\frac{(P_{O_2})_E}{(P_{Na})_E^3} = \frac{K_7}{(P_{Na})_E^3} = \frac{(P_{Na})_D^3 (P_{O_2})_D}{(P_{Na})_E^3}$$

The solid phases in all of the above reactions are assumed to have unit activity and to have the molecular formulas as written. Also, it is obvious that errors in the measured partial pressures of Na(g) and O_2 in region A will be compounded in these calculations; thus, these values must be accurately determined.

Partial pressures of O_2 were calculated for the three-phase region UO_2 -Na- Na_3UO_4 using the procedure outlined above.* The values calculated at 1000 and 1200°K are 3.30×10^{-35} and 1.61×10^{-27} atm, respectively, which correspond to O/M ratios of 1.95 and 1.96 for the mixed oxide 80 mol % UO_2 -20 mol % PuO_2 . The oxygen partial pressures for these O/M values were taken from the data of Rand and Markin.² For a temperature of 1000°K, these results indicate that Na(l) will react with UO_{2+x} to form Na_3UO_4 and UO_2 when the P_{O_2} is greater than 3×10^{-35} atm and the converse is true when the P_{O_2} is less than 3×10^{-35} atm. At this temperature and oxygen pressure, the sodium would have an equilibrium concentration of 17 ppm oxygen. This value was calculated from equations presented by Kassner and Smith.³

B. U-Pu-O, Na-U-O and Na-U-Pu-O Phase Studies (A. E. Martin, F. C. Mrazek)

The U-Pu-O phase study was discontinued temporarily so that a greater effort could be given to the Na-U-O and Na-U-Pu-O phase studies. The latter are of great importance in the operation of sodium-cooled fast reactors because of the possible reaction of coolant with the fuel in the event of a rupture in the fuel cladding. The severity of the problem may determine how long failed fuel elements can be stored in the reactor core and also whether or not failed fuel elements can be stored in the sodium coolant in the reactor.

1. The Na-U-O Phase Study

Although, in relation to fast-reactor fuels, the study of the Na-U-Pu-O system is the primary need, a concurrent study of the Na-U-O system is being made because such a study can be carried out in non-plutonium gloveboxes and because the experimental techniques which are developed can be applied later to a study of the Na-U-Pu-O system.

As was reported previously,⁴ we had confirmed the observations of Pepper *et al.*⁵ that Na_3UO_4 was the only Na-U-O phase which can exist in equilibrium with UO_2 and sodium. Our tests were at 750 and 800°C. In effect, we had identified a composition triangle in the Na-U-O system,

* For region E, the P_{Na} was assumed to be equal to that of pure sodium (experimental results indicate this to be true).

namely, $\text{UO}_2\text{-Na-Na}_3\text{UO}_4$. Additional composition triangles have since been established by reacting various mixtures of uranium dioxide, U_3O_8 , Na_2O , and sodium in sealed nickel capsules and identifying the phases present in the products by X-ray diffraction examination. In this way, the following composition triangles, at the temperatures indicated, were established: $\text{NaUO}_3\text{-Na}_3\text{UO}_4\text{-UO}_2$, 800°C; $\text{NaUO}_3\text{-Na}_3\text{UO}_4\text{-Na}_4\text{UO}_5$, 800 and 900°C; and $\text{NaUO}_3\text{-Na}_4\text{UO}_5\text{-Na}_2\text{UO}_4$, 950°C.

As was reported in ANL-7775, the compound Na_3UO_4 had previously been prepared successfully as a single-phase material on a 2-g scale. Several preparations (see Table I-1) have now been made on a 70-g scale to provide sufficient material for the establishment of the thermodynamic properties of Na_3UO_4 by other groups in the Division. The preparation procedures varied to some degree. The procedure used for preparation of FS-56 (Table I-1) was as follows. Mixtures of Na_2O and $\text{UO}_{2.14}$ were ground together and added to a nickel capsule containing sodium. The capsule was welded shut in a helium-atmosphere glovebox. The capsule was heated at 900°C for 18 hr, cooled to room temperature, inverted, heated to 600°C for 1 hr, reinverted, heated at 900°C for 18 hr, and cooled to room temperature. The capsule was cut open and then heated at 400°C in vacuum for 20 hr to remove the free sodium. The product was a powder of a uniform brown color.

Data on this preparation and two others are given in Table I-1. Included are the sodium and uranium analyses, the X-ray analyses, and composition calculations based on the chemical analyses. Also included for comparison are corresponding data for theoretical Na_3UO_4 .

The X-ray examination showed Na_3UO_4 to be the major phase in each of the preparations. Two preparations contained an additional phase, either UO_2 or NaUO_3 , at about the detection limit.

Samples of the three products were sintered in sealed nickel capsules at 1275°C and examined metallographically. In each case, the phases observed were the same as were detected in the X-ray examinations.

Within the accuracy of the analyses, the data of Table I-1 are considered to verify the experimental evidence obtained by Pepper *et al.*⁵ that the formula of the Na-U-O phase that can exist in equilibrium with UO_2 and sodium is Na_3UO_4 .

The X-ray diffraction data for the Na_3UO_4 phase in most of our preparations, including the three listed in Table I-1, contain many weak lines not reported by Pepper *et al.* When only the strong lines are considered, the data can be indexed as a simple face-centered cubic (fcc) structure with a lattice parameter of 4.78 to 4.79 Å, in agreement with Pepper *et al.* However, Na_3UO_4 presumably has a more complicated structure as evidenced by the fine lines of its pattern. The overall X-ray data which we obtained for Na_3UO_4 agree well with X-ray data reported by Bartram and Fryxell⁶ for an Na-U-O phase which they had obtained by reactions of uranium dioxide with sodium carbonate. (They had deduced this phase to be $\text{Na}_{11}\text{U}_5\text{O}_{16}$, but not on chemical evidence, since they had been

Table I-1. Data on Preparations of Na_3UO_4

	Preparations			Na ₃ UO ₄ (Theoretical)
	FS-53	FS-55	FS-56	
Chemical Analyses (wt %)				
Free sodium	--	<5 x 10 ⁻⁴	<5 x 10 ⁻⁴	0
Total uranium	64.6	63.6	65.0	64.15
U ⁴⁺ a	33.7	28.7	29.0	32.07
U ⁶⁺ (by difference) ^a	30.9	34.9	36.0	32.07
Na	18.1	18.2	17.9	18.60
Calculations from Chemical Analyses (Mole ratios)				
U ⁶⁺ /U ⁴⁺ a	0.9169	1.216	1.241	1.000
Na/(U + Na)	0.7436	0.7476	0.7403	0.7500
O/(U + Na)				
(from O by difference)	1.022	1.075	1.017	1.000
O/(U + Na)				
(from O obtained by credit- ing oxygen to U ⁶⁺ , U ⁴⁺ , and Na ⁺)	1.007	1.017	1.033	1.000
X-ray Diffraction Results				
Major phase	Na ₃ UO ₄	Na ₃ UO ₄	Na ₃ UO ₄	
Minor phase	UO ₂ at about detection limit	NaUO ₃ , one line of pattern	None	

^aThe Na_3UO_4 sample was dissolved in an aqueous solvent, and under the conditions used, U^{5+} formed an equal mixture of U^{4+} and U^{6+} (UO_2^{++}).

unable to produce it as a single-phase material. Apparently, they had unknowingly produced Na_3UO_4 .) Until the structure of Na_3UO_4 has been worked out, it will be convenient to continue representing its structure as fcc, based only on the strong lines of its X-ray pattern.

2. The Study of the Na-U-Pu-O System

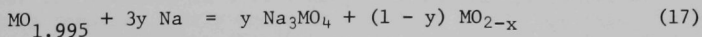
The study of the Na-U-Pu-O system has not progressed as far as that of the Na-U-O system. As was previously reported (ANL-7775), the Na-U-Pu-O phase, which can exist in equilibrium with a 20 mol % PuO_2 -80 mol % UO_2 powder and sodium at temperatures of from 800 to 950°C, was established as Na_3MO_4 , i.e., $\text{Na}_3(\text{Pu}_y\text{U}_{1-y})\text{O}_4$, by X-ray examination of equilibration products. The information here reported is on the reaction of sintered mixed-oxide pellets with sodium.

Sintered mixed-oxide pellets [O/M = 1.995, $\text{Pu}/(\text{U} + \text{Pu}) = 0.20$, percent of theoretical density = 90.1] were reacted with liquid sodium at 900°C in welded-shut nickel capsules for various periods up to 20 days. The capsules were then cut open and the free sodium was removed, either by vacuum treatment at 450°C or by dissolution in ethyl alcohol. The pellets were then weighed and measured.

Portions of the product pellets were mounted in polyester resin by vacuum impregnation, ground and polished (using kerosene as a lubricant), and examined metallographically. As can be seen in Fig. I-2, the product of the reaction of sodium with the mixed-oxide phase was readily distinguished as a gray phase somewhat darker than the mixed-oxide phase. This reaction product was present as a discontinuous layer on the outside surface of the pellets, as bands at and near cracks in the pellets, and as a grain-boundary phase in the same areas.

In order to identify the reaction-product phase, X-ray samples were taken from one pellet, which had been reacted with sodium for two days at 900°C. One sample was taken by scraping the surface, and one sample was taken from the interior of the pellet. The X-ray examination showed both samples to contain the two phases, Na_3MO_4 and MO_2 . Na_3MO_4 was the major phase in the surface sample and the minor phase in the interior sample. Thus, the reaction-product phase was identified as Na_3MO_4 , and the result of the equilibration study, mentioned above, was confirmed.

The weight increases for three pellets, which had been reacted with sodium for 1, 7, and 20 days at 900°C, were 0.48, 0.53, and 0.60%, respectively. Based on the weight increases, the O/M compositions of the product mixed-oxide phase were calculated to be 1.957, 1.953, and 1.947, respectively. For these calculations, it was assumed (1) that the sodium, which contained only 4 ppm oxygen, was a negligible source of oxygen for the formation of Na_3MO_4 and (2) that the reaction which occurred was as follows:



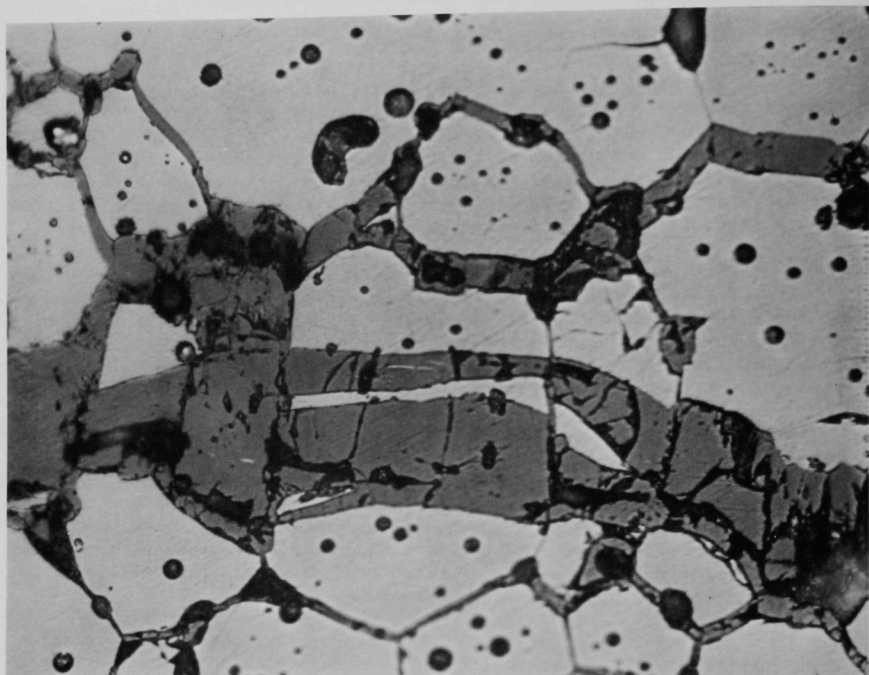


Fig. I-2. Na_3MO_4 Phase Formed from Reaction of 20% PuO_2 -80% UO_2 Sintered Pellet with Liquid Sodium at 900°C for 2 days. As polished, 700X. ANL Neg. No. 308-2571.

Light Gray Phase = Mixed-Oxide Phase
Intermediate Gray Phase = Na_3MO_4
Dark Gray and Black Areas = Porosity

Thus the calculations suggest that most of the reaction had occurred during the first day and that the final O/M composition was about 1.95.

Several of the pellet products of the reaction with sodium at 900°C and several sintered pellets of Na_3UO_4 have been prepared for examination with an electron probe microanalyzer (EPM). The final step in the preparations consists of evaporating a protective coating of gold onto the specimens. Methods for EPM examinations are still under development; optimum conditions of sample preparation and optimum EPM operating conditions are being sought. In some instances, steady signals for uranium, sodium, and oxygen have been obtained on sintered pellets of Na_3UO_4 . To date, the signals from the Na_3Mo_4 phase in the reaction products have been more erratic.

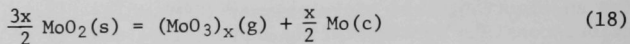
C. Studies of the U-Mo-O System (I. Johnson, P. M. Danielson)

The chemistry of the U-Mo-O system is being investigated to provide a basis for understanding the extensive migration of molybdenum that has been observed in the post-irradiation examination of oxide fuels. The migration of molybdenum during irradiation is believed to be related to the local values of the oxygen potential and the temperature. Furthermore, the migration of volatile molybdenum oxides under the temperature gradient in the fuel will redistribute the oxygen in the fuel matrix; this process would be of major significance in high-burnup fuels. In the present investigation, the partial pressures of the gaseous molybdenum oxide species in equilibrium with UO_2 - MoO_2 mixtures are being determined as a function of the O/M ratio and the temperature. A Knudsen effusion-mass spectrometry method is being used for these studies. The experimental apparatus was described previously.⁷

Preliminary experiments were done to determine the general nature of the interaction of molybdenum oxide with hyper- and hypostoichiometric urania. Samples of MoO_2 , $\text{UO}_{2.08}$ -10 wt % MoO_2 and $\text{UO}_{1.96}$ -10 wt % MoO_2 were heated in an iridium-lined Knudsen effusion cell, and the vapor species and their relative concentrations estimated by mass spectrometry. In all cases, MoO_2 , MoO_3 , $(\text{MoO}_3)_2$, and $(\text{MoO}_3)_3$ were formed in the gas phase effusing from the Knudsen cell. The total pressure of molybdenum oxide species was greatest over the $\text{UO}_{2.08}$ -10 wt % MoO_2 mixture and least over the $\text{UO}_{1.96}$ -10 wt % MoO_2 mixture. For each mixture and for pure MoO_2 , the order of decreasing partial pressures was found to be MoO_3 , $(\text{MoO}_3)_2$, MoO_2 , and $(\text{MoO}_3)_3$.

A more detailed study is under way on the interaction of molybdenum oxide with hypostoichiometric urania. In the first experiments in this study, a mixture of $\text{UO}_{1.96}$ and MoO_2 was first equilibrated in a closed Knudsen cell at about 1693°K for 2 hr, and then the equilibrium vapor composition was determined as a function of time at constant temperature. It was found that the partial pressures of the four molybdenum oxide gaseous species decreased slowly to nearly constant values as the effusion proceeded. The partial pressure of gaseous MoO_3 (and its polymers) decreased relatively more rapidly than that of gaseous MoO_2 . The experiment was done by successive additions of 2, 2, and 4 wt % MoO_2 to a sample of $\text{UO}_{1.96}$. The pressure-versus-time behavior for the three effusion periods were similar except that, after the addition of 4 wt % MoO_2 , the partial pressures of the gaseous species remained nearly constant for about 90 min and then decreased to about the same values observed at the end of the two 2-wt %

additions. From the weight loss of the samples and the average composition of the vapor, the overall composition of the samples at the end of the effusion stage was estimated. If it is assumed that MoO_3 and its polymers are formed by the disproportionation reactions



then the composition of the oxide phase can be computed. The overall composition of the oxide phase was computed to be $\text{U}_{0.96}\text{Mo}_{0.04}\text{O}_{1.97}$ at the end of all three effusion steps. X-ray examination of the residue confirmed that metallic molybdenum was present. The lattice constant of the fluorite phase in the residue was slightly smaller than that for stoichiometric urania. From the ratio of the partial pressures of MoO_2 and MoO_3 in the gas phase at the end of the effusion stage and from thermodynamic data,⁸ the oxygen potential ($RT \ln P_{\text{O}_2}$) was estimated to be -81 kcal/mol (at 1693°K). If the residue were a mixture of pure MoO_2 , Mo, and urania, the oxygen potential should be that of the Mo-MoO₂ system, which at this temperature is about -71 kcal/mol .⁸ The significantly lower value found in this experiment suggests that the molybdenum oxide interacts with the urania so as to lower its activity. If this preliminary result is confirmed, it suggests that the partial oxidation of fission product molybdenum may occur in a mixed urania-plutonia fuel at a lower oxygen potential than that of the Mo-MoO₂ system. This would have the effect of buffering the oxygen potential of the fuel.

D. Studies of the U-Pu-O System Containing Fission Products (I. Johnson, D. V. Steidl)

The chemistry of the Pu-U-Cs-O system is under investigation to provide a factual basis for understanding the interaction of fission-product cesium with the UO_2 -PuO₂ fuel matrix under reactor operational conditions. The interaction of cesium with the fuel matrix appears to be important in the determination of the extent of cladding attack and the magnitude of solid-fuel swelling. In the present investigation, the activity of cesium in a mixed UO_2 -PuO₂ matrix will be determined as a function of composition and temperature. The cesium activity is expected to be significantly dependent on the oxygen potential of the system, the cesium content of the solid phases, the nature (structure) of the solid phases, and the temperature.

To gain a rapid insight into the interaction of cesium with a typical fuel oxide, the initial experiments are being conducted using urania as a stand-in for the mixed uranium-plutonium oxide. Samples of the U-Cs-O system have been prepared by heat treatment of mixtures of urania, cesium oxide, and cesium metal in sealed capsules. The phases present in the samples after heat treatment are being determined by X-ray diffraction analysis. The vapor compositions over selected samples are being determined as a function of temperature by Knudsen effusion-mass spectrometry.⁴ The results of a series of sample-preparation experiments are given in Table I-2. These results are used to construct the partial phase diagram shown in Fig. I-3. The exact stoichiometry of the urania in equilibrium with the cesium uranate and cesium or the range of stoichiometry of the cesium uranate has not been determined. In the effusion-mass spectrometry studies of Samples 1 and 3, it was found that cesium was the principal

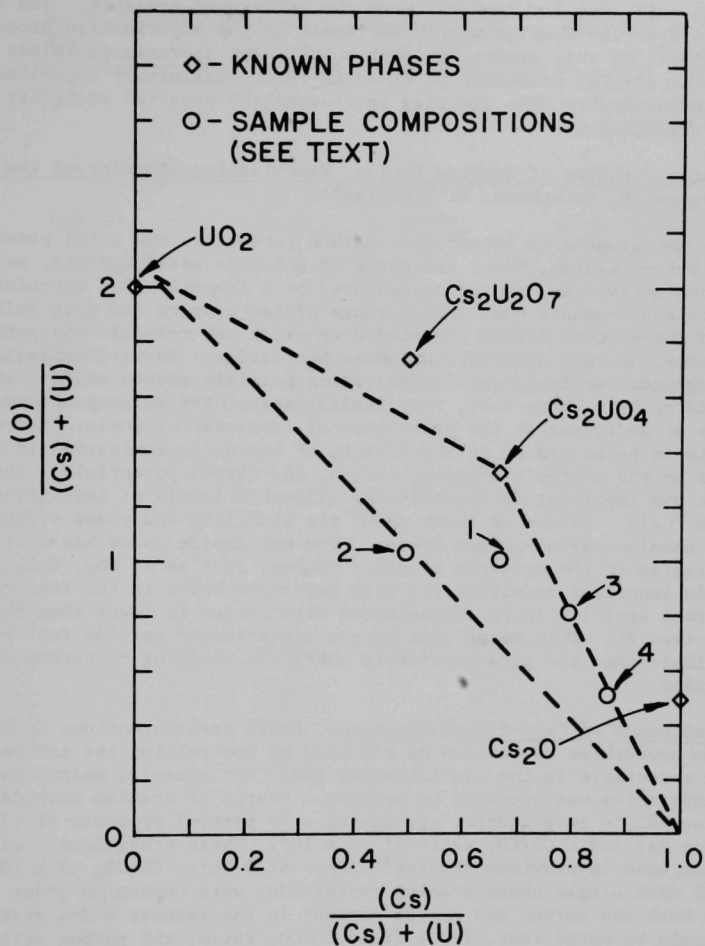


Fig. I-3. Partial Phase Diagram of U-Cs-O System

species which could be unambiguously assigned to the gas phase over the sample. Oxygen was also found in the gas phase; however, the partial pressure of oxygen in the ionization chamber, which originated from the effusion cell, was low compared with the background pressure. The cesium pressure over the samples slowly decreased as the vaporization proceeded. Measurements on this system are continuing. The approximate values of the cesium partial pressures obtained in these preliminary experiments are somewhat higher than expected in view of the reported stability of cesium uranate.⁹

E. Thermodynamics of Carbide Fuels: Vaporization Behavior of the U-C-O System (M. Tetenbaum, W. Nakajima*)

In the program to investigate carbon potentials and total pressures of the U-Pu-C system, total pressures of actinide metal species, as well as carbon activities, are being measured by a transpiration technique. Activity measurements over a wide range of temperature and with well-defined phase compositions are needed to establish reliable thermodynamic quantities, as well as to define phase boundaries. In particular, carbon-activity data are important in predicting possible carbon embrittlement of cladding by carbide fuel, the chemical state of fission products, and effects of additives on the properties of fast-reactor fuels. Current emphasis is being placed on the effects of oxygen contamination in uranium carbide on the system's uranium, carbon, and oxygen potentials. These studies are important in establishing allowable levels of impurities in carbide fuels. Little is known about the stability and phase relations of the uranium-carbon-oxygen system. The oxycarbide phase has mostly been investigated in the presence of other phases, such as U, UO_2 , U_2C_3 , and UC_2 . An important result of the work described below is the finding that the carbon activity in UC contaminated with oxygen is lower than that of oxygen-free UC. This means that oxygen-contaminated carbide fuel would be less likely than the pure carbide to embrittle cladding by carbon contamination.

Influence of Oxygen Contamination. Phase transformations in the uranium oxycarbide system can be effected by controlling the carbon and oxygen potentials in the equilibrating gas. For example, multiphase uranium oxycarbide was prepared by heating a charge of uranium carbide ($\text{C/U} = 0.95$) at 2020°K in a carrier gas having a CO partial pressure of ~ 75 Torr (balance He) and a CO/CO_2 ratio of $\sim 7 \times 10^3$. These conditions, relative to those used in previous studies¹⁰ ($P_{\text{CO}} \sim 4$ - 10 Torr, $\text{CO/CO}_2 \sim 4 \times 10^4$, $T = 2355^\circ\text{K}$) with single-phase uranium oxycarbide, were chosen in order to increase both the carbon and oxygen content in the ternary U-C-O system. (It should be noted that, for a fixed CO/CO_2 ratio, the carbon activity increases with decreasing temperature.) In addition, we wanted to establish whether the results of our oxygen partial-pressure measurements¹¹ over urania compositions were consistent with establishing conditions for pre-

* Resident Associate from Power Reactor and Nuclear Fuel Development Corp., Ibaraki, Japan.

Table I-2. Reactions of Cs_2O and Cesium with Urania

Expt. No. ^a	Initial Composition, millimoles			Phases Found (X-ray)	Behavior on Heating in Vacuum
	UO_2	Cs	Cs_2O		
1	3.59	-	3.55	Cs_2UO_4 , UO_2	Cs in vapor, Cs_2UO_4 disappeared
2	2.67	2.64	-	UO_2	
3	0.59	-	1.13	Cs_2UO_4	Cs in vapor, Cs_2UO_4 disappeared, UO_2 formed
4	0.61	1.74	1.17	Cs_2UO_4	

^aHeat treatment given samples. Expt. No. 1: 727°C, 75 hr. Expt. No. 3: 720°C, 6 days. Expts. No. 2 and 4: 720°C, 6 days; capsule opened, heated in vacuum at 290°C for 3 days.

dicting the formation of $\text{UO}_2(\text{s})$ in uranium carbides; i.e., to form $\text{UO}_2(\text{g})$, the oxygen partial pressures must be greater than that needed for the formation of $\text{UO}_2(\text{s})$. It should be noted that in order to avoid the formation of $\text{UO}_2(\text{s})$, the oxygen partial pressure must be lower than that needed for the formation of $\text{UO}_2(\text{s})$. The CO/CO_2 ratio of $\sim 7 \times 10^3$ yields a calculated value of $\log P_{\text{O}_2} (\text{atm}) = -13.18$ at 2020°K . From our oxygen partial pressure measurements, $\log P_{\text{O}_2} (\text{atm}) = -14.85$ over stoichiometric urania. Metallographic as well as X-ray examination of the residues showed the presence of $\text{UO}_2(\text{s})$ as well as " UC " and " UC_2 ". The formation of $\text{UO}_2(\text{s})$ is consistent with expectations. The gross composition of the residues was $\text{UC}_{1.07}\text{O}_{0.81}\text{N}_{0.01}$ after equilibration with the carrier gas for 24 hr. From the CO/CO_2 ratio, the calculated carbon activity (a_{C}) at 2020°K is 0.015, whereas the carbon activity value estimated from our measurements¹² with $\text{H}_2\text{-CH}_4$ mixtures over "oxygen-free" $\text{UC}_{1.07}$ was about 0.8-0.9 at 2020°K . Consistent with previous observations, it appears that the dissolution of oxygen in the carbide lattice decreases the activity of carbon in this system. Since the oxycarbide composition was hyperstoichiometric with respect to carbon, this reduction in carbon activity can have important implications in the transfer of carbon from fuel to cladding materials.

The question arose whether conditions could be adjusted so that the removal of UO_2 and UC_2 from the multiphase residue could be attained. We could proceed by two paths, (1) by changing the CO/CO_2 ratio so that the value of the oxygen partial pressure would be less than that required to form $\text{UO}_2(\text{s})$ at 2020°K , or (2) by increasing the temperature and maintaining the same CO/CO_2 ratio used to form the multiphase residue. The latter procedure was chosen for our exploratory investigation. The multiphase residue was heated for ~ 12 hr at 2355°K in a carrier gas having a CO/CO_2 ratio of $\sim 7.6 \times 10^3$ and a CO partial pressure of ~ 72 Torr (balance He). Under these conditions, $\log P_{\text{O}_2} (\text{atm}) = -11.20$ and $a_{\text{C}} = 3.4 \times 10^{-3}$. From oxygen partial pressure measurements¹¹ over stoichiometric urania, $\log P_{\text{O}_2} = -11.04$ at 2355°K . Metallographic analysis of the residue revealed a uniform structure containing UC as the major phase, a small amount of Widmanstätten UC_2 precipitate* within the UC grains, and, in addition, what appears to be a very fine Widmanstätten precipitate along the grain boundaries. UO_2 was not observed; X-ray examination showed UC only. The composition of the residue was $\text{UC}_{0.87}\text{O}_{0.09}\text{N}_{0.02}$, as determined from carbon, oxygen, and nitrogen analysis (uranium by difference). It should be noted that the oxygen content was reduced from ~ 28 at. % in the multiphase residue containing UO_2 to ~ 4.4 at. % in the UO_2 -free final residue. The results are summarized in Table I-3 and in Fig. I-4, which shows the phase fields traversed during these runs. It is apparent from the phase diagram, proposed by Henry *et al.*,¹³ that the composition of the final residue falls in the single-phase UC_xO_y region, which is consistent with the observations based on metallographic and X-ray analysis. It is also apparent that we are able to effect phase transformations in the U-C-O system by means of controlled carbon and oxygen potentials in the equilibrating carrier gas stream.

* Widmanstätten precipitate (UC_2) indicates the presence of a high-temperature solid solution of monocarbide and dicarbide that precipitated upon cooling.

Table I-3. Composition and Phase Transformation Traverse via Controlled Oxygen and Carbon Potentials in Carrier Gas

Designation on Ternary Phase Diagram ^a	T, °K	Heating Time, hr (cumulative)	Phases Found		Gross Composition
			Metallographic Examination	X-ray Examination	
○ (starting material)	-	-	UC	UC	UC _{0.95} ^O 0.002 ^N 0.006
▽	2020	16.6	UC, UC ₂ , UO ₂	UC, αUC ₂ , UO ₂	UC _{1.01} ^O 0.14 ^N 0.01
□	2020	24	UC, UC ₂ , UO ₂	-	UC _{1.07} ^O 0.81 ^N 0.01
●	2355	12	UC Wid. UC ₂	UC only	UC _{0.87} ^O 0.09 ^N 0.02

^aSymbols designate compositions in Fig. I-4.

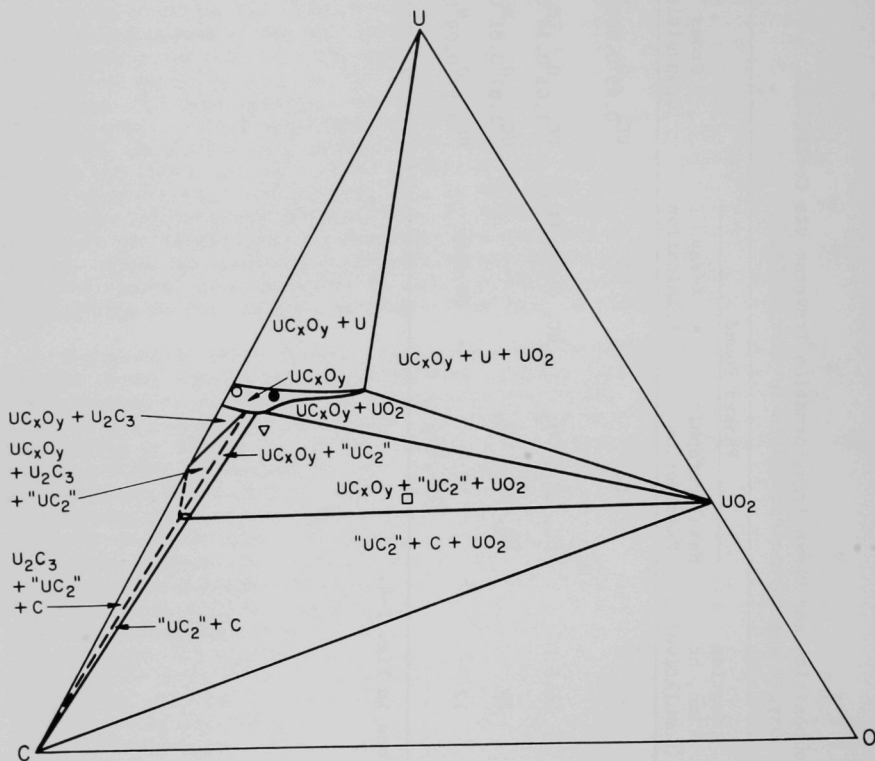


Fig. I-4. Tentative Phase Diagram of U-C-O System at $\sim 1700^\circ\text{C}$.
ANL Neg. No. 308-2655 Revised 1.

II. CHEMISTRY OF IRRADIATED FUELS AND MATERIALS (C. E. Johnson, C. E. Crouthamel)

The study of the chemical behavior of irradiated fast-reactor fuels has as its principal objective the collection of chemical data that will aid in understanding the complex chemical processes that take place in these fuels during irradiation. The current effort has been concentrated on the distribution of fission product cesium and krypton and fuel-cladding reactions in irradiated mixed-oxide fuels.

A. Fission-Product Distribution in Mixed-Oxide Fuels (C. E. Johnson, G. E. Staahl)

1. Radial Distribution of Krypton

The expansion of fuel elements due to the accumulation of fission gas has long been recognized as a potential limitation to the burnup attainable in reactor fuels. Thus, information on the retention of fission gases in irradiated fuels is important in understanding the parameters that affect fuel swelling. Data have been obtained on the distribution of ^{85}Kr in a cross section of vibratorily compacted fuel of UO_2 -20 wt % PuO_2 . The sample, HOV-15, had an average density of 79.8% of theoretical and had been irradiated to 3.5 at. % burnup at a maximum linear power rating of 21.4 kW/ft.

Laser-beam vaporization was used to release the krypton contained in a small sample of the fuel. This technique has been described previously (ANL-7775, Section IV.A, in press). The procedure is briefly as follows: The sample is placed in a glass-covered vacuum chamber and the laser focused on a selected area. The chamber is evacuated, inactive krypton carrier gas is charged to the system, and the laser is fired. The released krypton and carrier gas are cryogenically pumped through a filter and a measured portion of the gas is taken for beta counting. The volumes of the craters produced when the samples are vaporized are determined from measurements of silicone rubber replicas of the specimen surface.

Laser samples were taken from representative areas of the fuel pin; namely, columnar grains, equiaxed grains, and unrestructured regions. The data for the radial distribution of ^{85}Kr , obtained in two separate experiments, are given in Fig. II-1. The data show good reproducibility throughout the sample. The low fuel density coupled with the high heat rate has created a fuel which consists primarily of columnar grains, with a relatively small volume occupied by the equiaxed grains and unrestructured region. The high concentration of krypton at the hot void edge suggests that pore migration toward the hotter end of the thermal gradient is occurring, with trapped gas bubbles accumulating at the void edge owing to the rapidly decreasing temperature gradient. Pore migration at the cooler ends of the columnar grains does not appear to lower the gas concentration as effectively as in the mid-columnar grain region. Gas retention in the equiaxed-grain region, where gas release is controlled predominantly by the progressive linkup of grain-boundary bubbles, is somewhat higher than in the mid-columnar grains, and retention is even higher in the unrestructured zone.

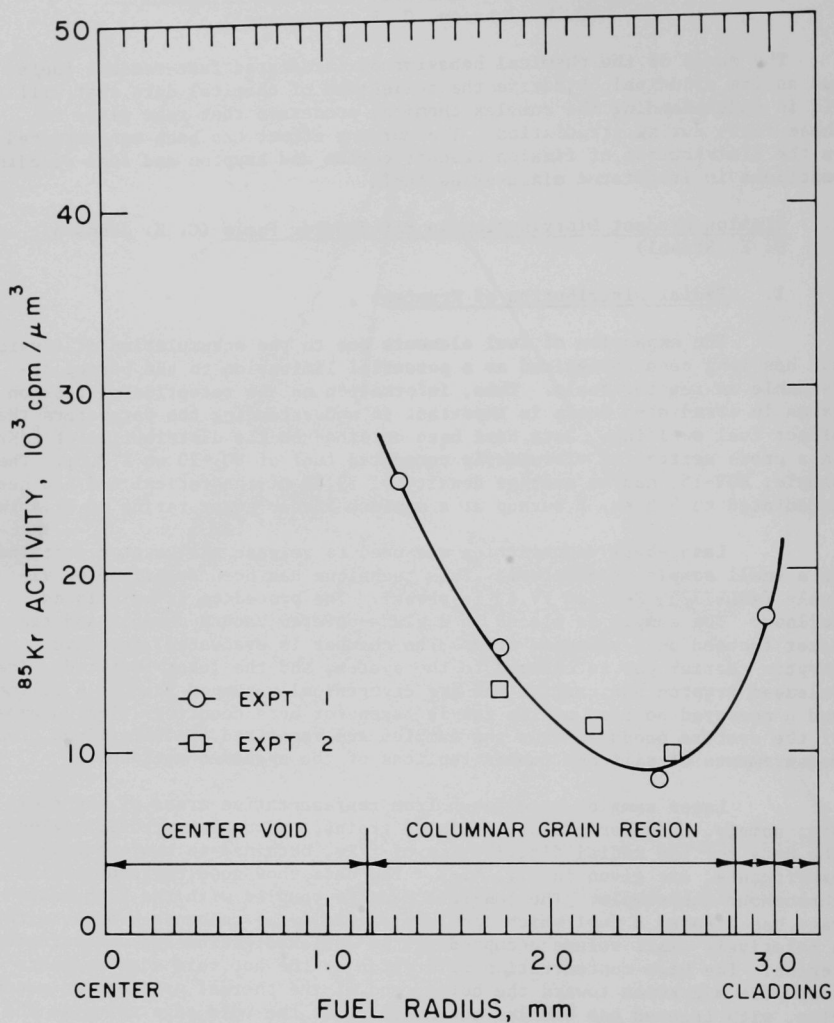


Fig. II-1. Radial Distribution of ^{85}Kr in Irradiated Mixed-Oxide Fuel (HOV-15)

The observed concentrations of ^{85}Kr in HOV-15 are about one-half of those observed for F2R (see ANL-7775). This correlates well with the reported fission-gas release data; for HOV-15 the release of fission gas was 82%,¹⁴ and for F2R the release was only 60.8%.¹⁵

2. Radial Distribution of Cesium

Measurements have also been made of the radial distribution of ^{137}Cs in fuel samples HOV-15, F2R, and SOV-6. These data were obtained by a combination of laser-beam vaporization and gamma-ray spectroscopy. In this method, material vaporized by the laser beam is condensed on a cover glass placed 1 mm above the sample surface. The cover glass is removed and the deposited material is counted using a calibrated Ge(Li) detector in conjunction with a multichannel analyzer system. The ^{144}Ce content of each sample was also determined to provide a means of normalizing the data (cerium does not migrate in oxide fuels).

The distribution data for ^{137}Cs are given in Fig. II-2. The fuel parameters thought to be important in comparing the distribution of ^{137}Cs in these fuels are fuel density and maximum linear power rate. For HOV-15, these are, respectively, 79.8% and 21.4 kW/ft; for F2R, 94.3% and 16.0 kW/ft; and for SOV-6, 83.5% and 17.0 kW/ft. HOV-15 and SOV-6 are vibrapacked fuels and F2R is a high-density pellet fuel. Figure II-2 clearly shows that the ^{137}Cs concentration increases logarithmically out to the fuel-cladding interface for the vibrapacked fuels. In contrast, the ^{137}Cs concentration in F2R peaks at a circumferential crack in the fuel which roughly coincides with the boundary between the equiaxed and unstructured fuel regions. Little cesium penetration of the cladding has occurred in this high-density fuel, whereas considerable attack has been noted in the lower density vibrapacked fuels.

The driving force for migration of ^{137}Cs is complex. Of importance is the free-energy gradient that is set up in the fuel due to the temperature and concentration gradients found. The extent of cesium interaction with the fuel, if such an interaction does occur, will be determined by the localized oxidizing potential. Vapor-phase diffusion in the large thermal gradient will be affected by the interconnected porosity of the fuel. In the dense fuel (F2R), which has a minimum of interconnected porosity, cesium does not migrate to the fuel-cladding interface in any appreciable amounts; however, in the vibrapacked fuels a greater interconnected porosity allows easier transport of cesium to the cladding. Further work is being undertaken to gain a fuller understanding of the migration behavior of cesium.

B. Fuel-Cladding Chemical Interactions (C. E. Johnson, C. A. Seils, K. E. Anderson)

Although a number of irradiated mixed-oxide fuel specimens have been examined for evidence of intergranular attack of stainless steel cladding, little is known concerning the correlation between intergranular attack and fuel-fabrication and reactor-operating parameters. However, the studies that have been made suggest that the principal parameters initiating and controlling the cladding attack are the oxidizing potential and the temperature at the inner cladding wall. Various studies of the effect of oxygen

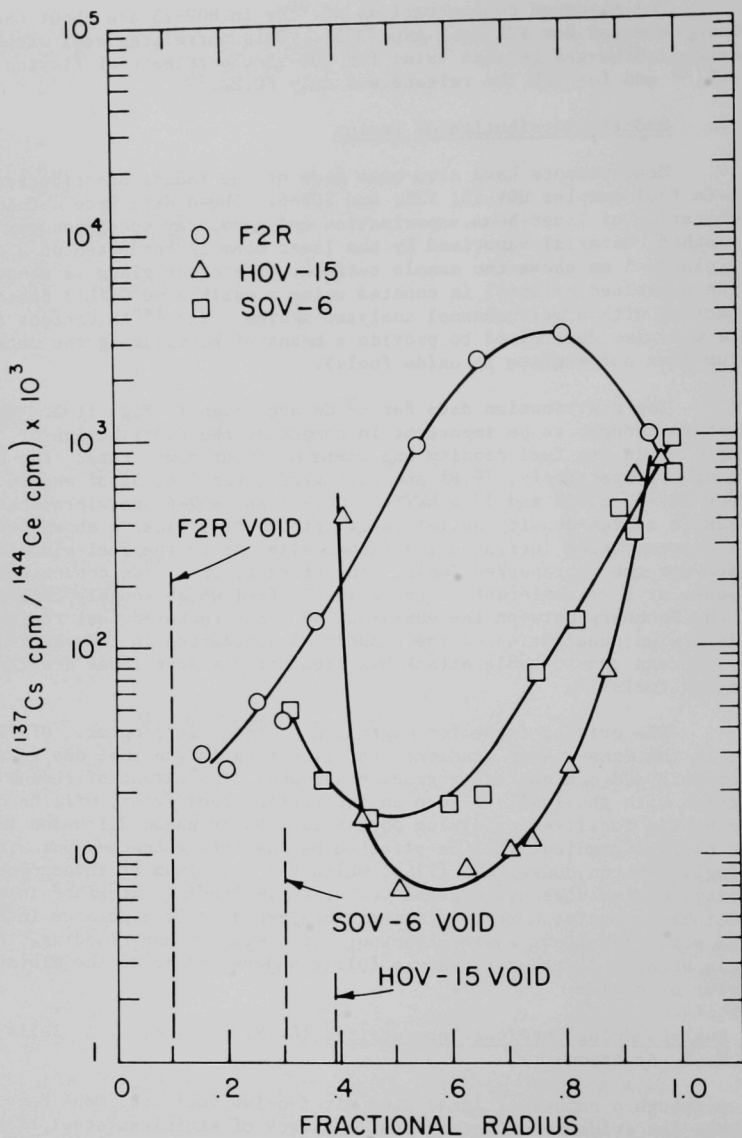


Fig. II-2. Radial Distribution of ^{137}Cs in Irradiated Mixed-Oxide Fuels

on the compatibility of alkali metals with stainless steels and refractory metals have shown that, in the presence of oxygen, the alkali metals (especially cesium) are capable of markedly accelerating corrosive attack on a wide variety of stainless steels and refractory metals.

Recent work in this laboratory has indicated that in irradiated mixed-oxide fuels the mechanism of attack of the cladding is oxidation at the grain boundaries. To assess this mechanism of intergranular attack further, small rings of cladding were selected from seven different irradiated fuels for oxygen analysis. The cladding sections were cut and flattened and scrupulously cleaned to assure complete removal of oxide fuel. Residual alpha activity was taken as an indication of whether or not fuel still adhered to the cladding. Cladding sections were considered to be ready for oxygen analysis only when they were completely free of alpha activity. At this point, each cladding section was divided into three segments and each segment was analyzed separately. The results of the analyses, which were performed by an inert-gas fusion technique, are given in Table II-1. All the samples of irradiated fuel cladding showed significantly higher oxygen contents than the unirradiated materials, which had oxygen contents of 50 to 97 ppm. Thus, it appears that the cladding is acting as an oxygen sink during irradiation. Oxygen may enter the cladding from the sodium side; however, the greater driving force is expected from the irradiated fuel. The variation in oxygen content among different segments of the same fuel cladding is larger than expected. Although this is believed to be a real effect, additional analyses would be required to establish the exact nature of this variation.

A section of cladding (SOV-1) was analyzed by gamma spectrometry using a Ge(Li) detector to determine the amount of fission product cesium located in the grain boundary region. Even with the assumption that cesium is present as $\text{Cs}_2\text{CO}_3 \cdot 2\text{H}_2\text{O}$ (which has the highest oxygen content of any species expected to be present), the cesium found accounts for 500 ppm oxygen, only a fraction of the total (3000 ppm) found. Thus, more oxygen is present in the bulk cladding than can be accounted for by the oxygen associated with cesium.

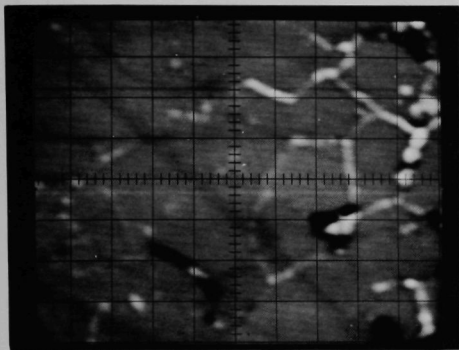
A section of cladding having the highest oxygen content (SOV-1, 45G14) was studied in detail with the electron microprobe by scanning areas $80 \mu\text{m}$ by $100 \mu\text{m}$. A rubidium acid phthalate diffraction crystal was used for oxygen analysis. X-ray images for oxygen, cesium, and molybdenum, obtained in an area $\sim 0.015 \text{ mm}$ from the fuel-cladding interface, are shown in Fig. II-3. The intergranular penetration in this area is evident.

This area of intergranular attack was further analyzed with the electron microprobe for oxygen, fission products, and cladding constituents by taking counts for each element at $1 \mu\text{m}$ intervals. These data are given in Fig. II-4. The data show an increase by a factor of four in the oxygen K_α counts in the grain boundaries. The most prominent and consistent features of intergranular attack were depletion of iron and chromium and enhancement of cesium, molybdenum, and oxygen. Although it is not apparent in Fig. II-4, previous studies of other areas of attack have frequently shown a migration of nickel to the grain boundaries leaving the intergranular areas with a higher nickel concentration than the bulk stainless steel.

Table II-1. Oxygen Content of Irradiated Stainless Steel Cladding
($^{235}\text{UO}_2$ -20 wt % $^{239}\text{PuO}_2$ fuels irradiated in EBR-II)

Sample Designation	Stainless Steel Cladding	Average Fuel-Pin Burnup, at. %	Peak Linear Power Rating, kW/ft	Inner Cladding Temp., °C	Intergranular Attack, mils	Fuel Density, % of Theor.	Oxygen Content, ^a ppm
SOV-1 (45G-14)	304	5.0	20	593	9	80	3300 3000 -
SOV-1 (45G-18)	304	5.0	20	530	2	80	1600 1300 870
C-11 (66A-11)	316L	9.5	14	530	0-1.5	88.3	1800 1800 -
C-15 (66B-7)	316L	9.5	13	525	0-1.5	82.7	2100 1300 -
SOV-6 (43B-25)	304	2.7	17	560	2	83.5	1100 470 420
007 (59B-20)	304L	4.7	15.7	567	0-2	84	610 560 -
F2R-3 (General Electric)	347	6.5	16.5	550	none	95	1600 940 740

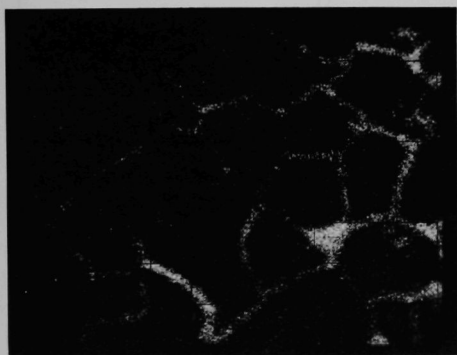
^aAnalysis of irradiated stainless steel cladding performed by Los Alamos Scientific Laboratory and Argonne by an inert-gas fusion technique.



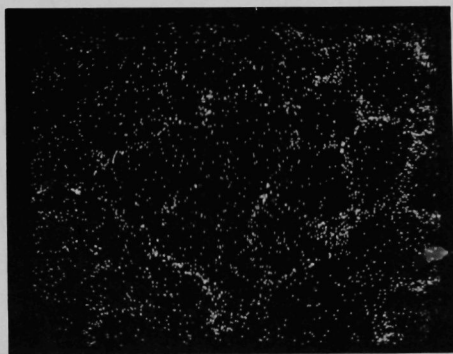
SPECIMEN CURRENT



MOLYBDENUM $L\alpha$



CESIUM $L\alpha$



OXYGEN $K\alpha$

Fig. II-3. Electron Microprobe Scanning Images of Irradiated Stainless Steel Cladding from SOV-1 (all images are 80 x 100 μm).
ANL Neg. No. 308-2480 T-1.

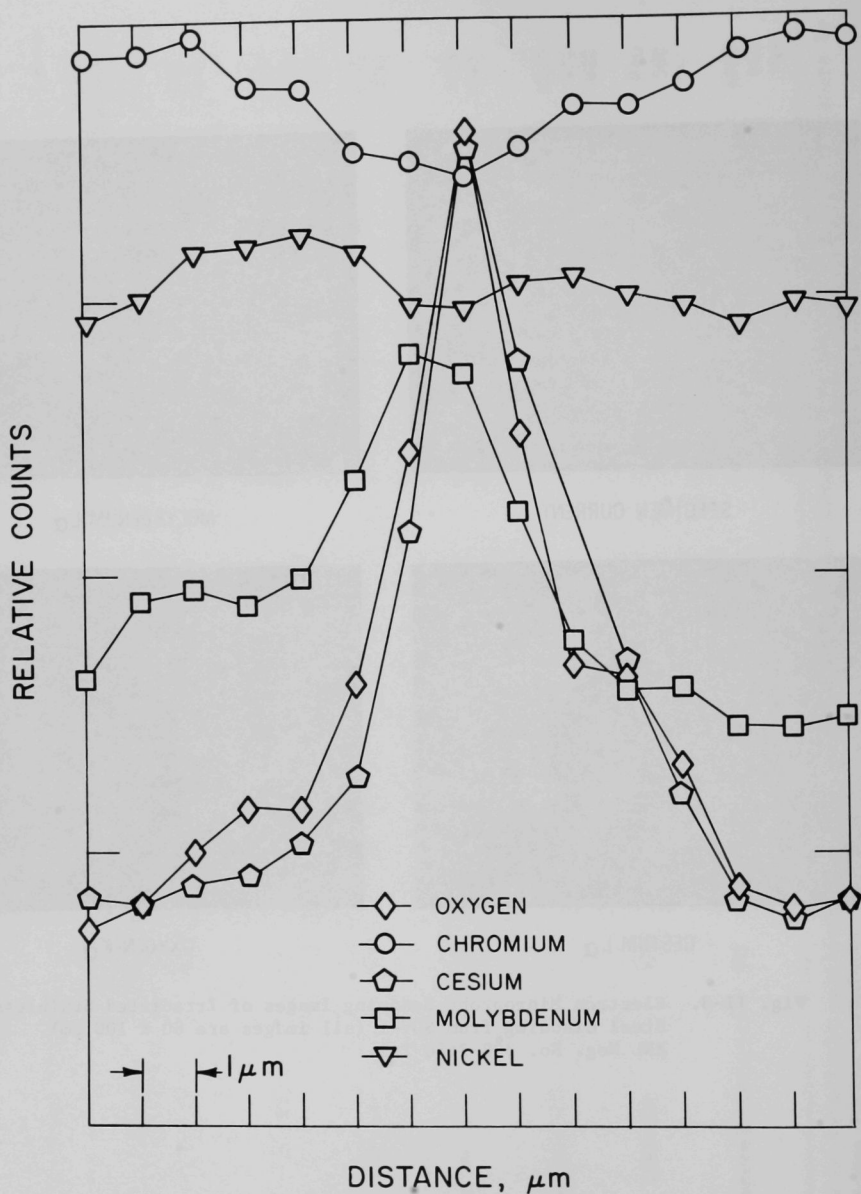


Fig. II-4. Electron Microprobe Analysis of an Area of Intergranular Attack in Irradiated Stainless Steel Cladding (SOV-1). ANL Neg. No. 308-2525.

It has been suggested¹⁶ that the intergranular attack may be proceeding by an induced, accelerated oxidation (similar to hot corrosion) of the stainless steel cladding. The hot-corrosion mechanism requires that a thin film of fused-salt electrolyte be condensed on the cladding surface and that the accelerated oxidation occur through this film. In irradiated fuels, condensation of an electrolyte is a real possibility. Although this electrolyte has not been identified, it might be an oxide mixture of fission products and possibly some cladding components. Relatively pure cesium oxide would not be thermodynamically stable at the oxygen potentials expected; however, the possibility exists for a lower oxygen activity for cesium oxide in a complex multicomponent electrolyte (e.g., Cs_2O , Cr_2O_3 , CsI , and iron, chromium, and molybdenum oxide species).

The presence of cesium and molybdenum in the intergranular areas gives substance to the hypothesis of corrosion through an electrolyte. In a study of the Cs_2O - MoO_3 system, Spitsyn and Kuleshon¹⁷ found a temperature minimum of 450°C for an equimolar mixture of Cs_2MoO_4 and MoO_3 . This temperature is well below the expected temperature of the cladding near the fuel-cladding interface. Furthermore, the oxygen activity at the cladding wall is a rapidly changing parameter near stoichiometric compositions of the fuel and an abrupt transformation of cesium from a metal to an electrolyte form would bring about an equally abrupt change in the corrosion conditions and probably establish the conditions necessary for cladding attack.

REFERENCES

1. J. E. Battles, W. A. Shinn, P. E. Blackburn, and R. K. Edwards, in Plutonium 1970 and Other Actinides, Proceedings of the Fourth International Conference on Plutonium and Other Actinides, Part II, pp. 733-742, AIME (1970).
2. M. H. Rand and T. L. Markin, "Some Thermodynamic Aspects of (U,Pu)O₂ Solid Solutions and Their Use as Nuclear Fuels," in Thermodynamics of Nuclear Materials, p. 637, IAEA, Vienna (1968).
3. T. F. Kassner and D. L. Smith, USAEC report ANL-7335 (1967).
4. Chemical Engineering Division Annual Report, 1970, USAEC report ANL-7775, Section III.A.3 (in press).
5. R. T. Pepper, J. R. Stubbles, and C. R. Tottle, Appl. Mat. Res. 3, 203 (1964).
6. S. F. Bartram and R. E. Fryxell, J. Inorg. Nucl. Chem. 32, 3701 (1970).
7. Chemical Engineering Division Annual Report, 1969, USAEC report ANL-7675, p. 80 (1970).
8. JANAF Thermodynamic Data, Dow Chemical Company, Midland, Michigan (June 30, 1967).
9. V. I. Spitsyn, Ed., Investigations in the Field of Uranium Chemistry, ANL-Trans-33, p. 170 (1961).
10. ANL-7675, p. 86 (1970).
11. M. Tetenbaum and P. D. Hunt, J. Chem. Phys. 49, 4739 (1968).
12. M. Tetenbaum and P. D. Hunt, High Temperature Thermodynamic Properties of Hypo and Hyperstoichiometric Uranium Carbides, J. Nucl. Mater. 40(1), 104 (1971).
13. J. L. Henry, L. P. Danton, R. Blickensderfer and H. J. Kelly, BMI-6968 (1967).
14. F. L. Brown *et al.*, Trans. Amer. Nucl. Soc. 12, 107 (June 1969).
15. W. E. Baily *et al.*, Proc. Int. Symp. on Ceramic Nuclear Fuels, p. 195, Amer. Ceram. Soc. (1969).
16. R. A. Rapp, Ohio State University, private communication (1971).
17. V. Spitsyn and I. M. Kuleshon, Zh. Obshch. Khim. 21, 1372 (1951).

8

ARGONNE NATIONAL LAB WEST



3 4444 00011584 0

